The 8th European Congress on Computational Methods in Applied Sciences and Engineering
ECCOMAS Congress 2022
5-–9 June 2022, Oslo, Norway

SIMULATING NONLINEAR ELASTIC BEHAVIOUR OF CABLES USING AN ITERATIVE METHOD

TIAN ZHAO[1,2], FABIO SCHNEIDER-JUNG[1], JOACHIM LINN[1] AND RALF MÜLLER[2]

[1] Fraunhofer Institute for Industrial Mathematics ITWM
Fraunhofer Platz 1, 67663 Kaiserslautern, Germany
e-mail: [tian.zhao, fabio.julian.schneider-jung, joachim.linn]@itwm.fraunhofer.de

[2] Technical University of Darmstadt
Franziska-Braun-Straße 7, 64287 Darmstadt, Germany
email: ralf.mueller@mechanik.tu-darmstadt.de

Key words: Nonlinear-elastic Behaviour, Cosserat Rod, Inverse Problem

Abstract. This contribution introduces a novel approach to simulate the nonlinear elastic bending behaviour of cables. Bending tests on real cables with complex structures clearly show the existence of nonlinear constitutive bending behaviour. In our current framework, only constant effective stiffness parameters are used. In order to enable nonlinear bending behaviour within the current framework, we propose an iterative method where, at each step, constant stiffness parameters are used and are updated according to the current cable state. The presented method is demonstrated by means of numerical experiments. Moreover, the inverse problem, i.e. the determination of state-dependent bending stiffness characteristic, is considered. Here, besides purely virtual considerations, we also investigate measurements from real cable experiments

1 INTRODUCTION

Flexible slender structures like cables and hoses are omnipresent in modern cars. Therefore, the demand of fast and geometrically exact simulations of these flexible objects has increased in recent years. In [1] and [2], typical applications of such a simulation tool are illustrated.

The theory of Cosserat rod provides a framework for modeling the deformation of cables in a geometrically exact and efficient way [2, 3, 4, 5]. We follow [2], where the static equilibrium of a Cosserat rod under given boundary conditions is obtained by minimization of the potential energy, which consists of the external potential (usually gravity) and the elastic energy. In many applications with rather simple cables and hoses, a linear elastic constitutive behaviour is sufficient, such that the elastic energy is characterized by constant effective stiffness parameters. However, for more complex cables, e.g. high-voltage cables or cable bundles, nonlinear constitutive bending behaviour can be clearly observed during cyclic pure bending [6] and MeSOMICS bending experiments [7]. Moreover, investigations taking into account inter layer friction and slip of cables, as the one conducted by Papailiou [8, 9], show the dependence between bending stiffness and bending curvature. Dörlich *et al.* used a piecewise linear elastic bending constitutive law to approximate the nonlinear elastic bending behaviour of a Bowden cable and applied it to Cosserat theory [6].

In this work, we propose an iterative method to enable nonlinear bending behaviour, namely a state-dependent bending stiffness characteristic, within the framework of energy minimization with constant stiffness parameters. The general idea is to iteratively update the constant stiffness parameters until the cable state converges. In each iteration, the constant stiffness parameters are set according to the current cable state and the new equilibrium is computed by energy minimization. Moreover, we discuss the inverse problem, i.e. how to determine the corresponding state-dependent bending stiffness characteristics from given measurement results.

The paper is structured as follows: Section 2 describes a Cosserat model in two-dimensional space. Next, the bending experiment used for our virtual and real experiments is introduced in Section 3. In Section 4, an iterative method is proposed which enables the simulation of nonlinear elastic behaviour, although in each iteration step, constant stiffness parameters are used for the energy minimization. The inverse problem is presented in Section 5, and we give a conclusion of our work in Section 6.

2 COSSERAT ROD IN TWO DIMENSIONAL SPACE

In this work, we only consider in-plane bending, therefore a simplified two-dimensional version of a geometrically exact Cosserat rod is used. The Cosserat rod is described by the centerline $(x(s), y(s))^T \in \mathbb{R}^2$ and the rotation angle $\alpha(s)$, with arc length parameter $s \in [0, L]$. Since we allow shear deformation, $\alpha(s)$ can be different from the centreline's tangent angle at arc length s. The rotation matrix at a given arc length can simply be represented as

$$\mathsf{R}(s) = \begin{pmatrix} \cos(\alpha(s)) & -\sin(\alpha(s)) \\ \sin(\alpha(s)) & \cos(\alpha(s)) \end{pmatrix}. \tag{1}$$

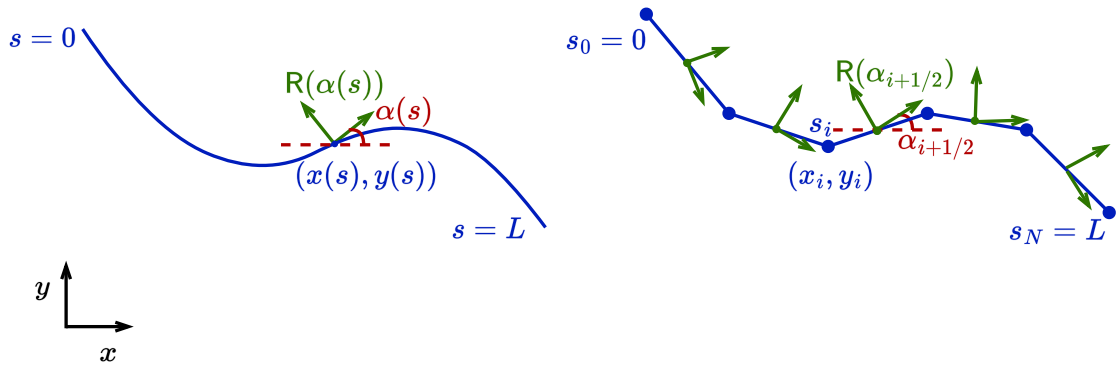

Figure 1: Left: Continuous Cosserat rod in $\mathbb{R}^2$. Right: Discrete Cosserat rod in $\mathbb{R}^2$.

2.1 Continuous Cosserat rod

In the continuous case, strain measures, i.e. the local bending curvature $K(s)$ and shear-extensional strain $\mathbf{\Gamma}(s)$ are given as

$$K(s) = \alpha'(s) \quad \text{and} \quad \mathbf{\Gamma}(s) = \begin{pmatrix} \Gamma_1(s) \\ \Gamma_2(s) \end{pmatrix} = \mathsf{R}(s)^T \cdot \begin{pmatrix} x(s) \\ y(s) \end{pmatrix}' - \begin{pmatrix} 1 \\ 0 \end{pmatrix}, \tag{2}$$

where $\Gamma_1(s)$ measures primarily extension and $\Gamma_2(s)$ measures transverse shearing.

Above we assumed vanishing pre-curvature in the undeformed rod configuration. In principle, one can incorporate a non-vanishing pre-curvature. However, in this work we consider only cases with a straight reference configuration.

For linear elastic rods, forces and bending moments can be formulated as $\mathbf{F} = \mathsf{C}_{\mathbf{\Gamma}} \cdot \mathbf{\Gamma}(s)$ and $M = [EI] \cdot K(s)$, where $\mathsf{C}_{\mathbf{\Gamma}} = \begin{pmatrix} [EA] & 0 \\ 0 & [GA] \end{pmatrix}$ contains the effective tension stiffness $[EA]$ as well as effective shear stiffness $[GA]$ and $[EI]$ is the effective bending stiffness. Finally, we can formulate the elastic potential energy as

$$W = \frac{1}{2} \int_0^L \mathbf{\Gamma}^T(s) \cdot \mathsf{C}_{\mathbf{\Gamma}} \cdot \mathbf{\Gamma}(s) ds + \frac{1}{2} \int_0^L [EI] \cdot K(s)^2 ds. \tag{3}$$

where the first term denotes the contribution of shear and tension energy, the second term is the bending energy. In principle, the static equilibrium can be obtained by minimizing the elastic potential energy. For more details, we refer to [2].

2.2 Discrete Cosserat rod

The configuration of a discrete Cosserat rod deformed in the x-y plane as shown in Fig. 1, consists of discrete vertices (x_i, y_i) and edge-centered rotation matrices $\mathsf{R}_i(\alpha_{i+1/2})$. The index i is used for vertex quantities at s_i for $i = 0, ..., N$ and $i + 1/2$ is used for edge-centered quantities at $s_{i+1/2}$ for $i = 0, ..., N-1$. The discrete local strains $\mathbf{\Gamma}_{i+1/2}$ are edge-centered quantities, while the discrete local curvatures K_i are vertex based quantities

$$\mathbf{\Gamma}_{i+1/2} = \mathsf{R}^T(\alpha_{i+1/2}) \cdot \begin{pmatrix} \frac{x_{i+1}-x_i}{\Delta s_{i+1/2}} \\ \frac{y_{i+1}-y_i}{\Delta s_{i+1/2}} \end{pmatrix} - \begin{pmatrix} 1 \\ 0 \end{pmatrix}, \quad K_i = \frac{\alpha_{i+1/2} - \alpha_{i-1/2}}{\delta s_i}, \tag{4}$$

where $\Delta s_{i+1/2} = s_{i+1} - s_i$ for $i = 0, ..., N$ and $2\delta s_i = \Delta s_{i-1/2} + \Delta s_{i+1/2}$ for $i = 0, ..., N-1$ ($2\delta s_0 = \Delta s_{1/2}$, $2\delta s_N = \Delta s_{N-1/2}$). Further details about the derivation from continuous case can be found in [10, 11].

The discrete approximation of the elastic potential energy using midpoint and trapezoidal quadrature is given as

$$V = \frac{1}{2} \sum_{i=0}^{N-1} \Delta s_{i+1/2} \cdot (\mathbf{\Gamma}_{i+1/2})^T \cdot \mathsf{C}_{\mathbf{\Gamma}} \cdot \mathbf{\Gamma}_{i+1/2} + \frac{1}{2} \sum_{i=0}^{N} \delta s_i \cdot [EI] \cdot K_i^2, \tag{5}$$

where the first term denotes the contribution of discrete shear and tension energy, the second term is the discrete bending energy. Again, the equilibrium state can be found by minimizing the elastic potential energy.

We want to emphasize, that the bending stiffness $[EI]$ might vary along the rod, such that we rewrite the potential bending energy from Eqn. (5) as

$$V_B = \frac{1}{2} \sum_{i=0}^{N} \delta s_i \cdot [EI]_i \cdot K_i^2 \tag{6}$$

with local bending stiffness $[EI]_i$ around each vertex s_i.

3 BENDING EXPERIMENT

Real bending experiments and virtual bending experiments are conducted to investigate the bending behaviour of cables.

3.1 Real bending experiment

Bending experiments are conducted on the MeSOMICS [7] measurement machine. In this bending experiment, the specimen is mounted between two low-friction bearings, such that we have (ideally) moment-free boundary conditions at both clamping points. Fig. 2 shows a top-view photo of the bending test. Fig. 3 shows a schematic sketch. During the test, the left clamping point is displaced stepwise towards the right clamping point, leading to different bending deformations (cf. Fig. 3), while the resulting reaction force at the right clamping point is measured and the applied displacement is recorded. The measured data is further used in Section 5.2 to determine the characteristic from the real bending experiment.

Figure 2: Top-view of MeSOMICS bending experiment.

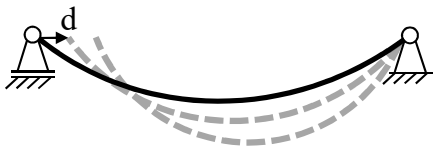

Figure 3: Schematic representation of experimental procedure for bending measurements.

3.2 Virtual bending experiment

Besides real bending experiments we also perform virtual bending experiments, using the discrete Cosserat rod in two-dimensional space from Section 2.1. The boundary conditions are the same as for the real bending experiment and we also, virtually, measure the resulting forces for the applied boundary conditions. The two-dimensional Cosserat rod is implemented using MATLAB and the built-in function `fmincon` is used to minimize the elastic potential energy. Fig. 4 shows an example of the bending deformations in virtual bending experiment.

4 ITERATIVE UPDATE OF CONSTANT BENDING STIFFNESS

As previously mentioned, during measurements we found that cables show nonlinear elastic behaviour, namely, a state-dependent bending stiffness. In this work, we focus on curvature-

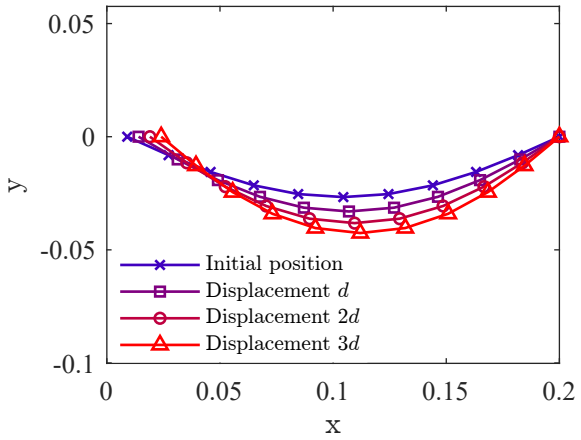

Figure 4: Bending deformations of the initial rod (already slightly bend) and three displacement steps d, $2d$, $3d$, with $d = 5 \cdot 10^{-3}\,\mathrm{m}$. The following parameters are used for the simulation: $L = 0.2\,\mathrm{m}$, $N = 11$, $[EI] = 10^{-3}\,\mathrm{Nm}^2$, $[EA] = 1000\,\mathrm{N}$, $[GA] = 1000\,\mathrm{N}$.

dependent bending stiffness parameters.

Following the work in [2], in general, the potential bending energy is $W_B = \int_0^L \Phi(K(s))ds$, where $\Phi(K(s))$ is the bending energy density. Again, the potential bending energy is discretized according to trapezoidal quadrature as $V_B = \sum_{i=0}^{N} \delta s_i \, \Phi(K_i)$.

The constitutive equation for the bending moment is given by

$$M(K(s)) = \left.\frac{d\Phi(K)}{dK}\right|_{K=K(s)}, \tag{7}$$

and, further, the local bending stiffness computes as

$$\left.\frac{dM(K)}{dK}\right|_{K=K(s)} = \left.\frac{d^2\Phi(K)}{dK^2}\right|_{K=K(s)} := f_{EI}(K(s)). \tag{8}$$

To make sure that an increased curvature always leads to an increased bending moment, the local bending stiffness must fulfill $f_{EI}(K(s)) > 0$ for all $s \in [0, L]$.

In general, $f_{EI}(K(s))$ also explicitly depends on the arc length s, such that the bending stiffness characteristic is different for all local cross sections. In this work, however, we only consider an implicit dependence of s via the bending curvature $K(s)$.

With $K_i = K(s_i)$, we find from Eqn. (7) and (8) that the local bending moment and the bending energy density can be written as

$$M(K_i) = \int_0^{K_i} f_{EI}(\kappa)d\kappa \quad \text{and} \quad \Phi(K_i) = \int_0^{K_i}\int_0^{\xi} f_{EI}(\kappa)d\kappa d\xi. \tag{9}$$

For the special case of a curvature-independent bending stiffness, i.e. constant $[EI]_i$ at each vertex, Eqns. (9) simplify to

$$M(K_i) = [EI]_i \cdot K_i \quad \text{and} \quad \Phi(K_i) = \frac{1}{2} \cdot [EI]_i \cdot K_i^2. \tag{10}$$

In principle, one can use the second Eqn. in (9) in the elastic potential energy to solve for the static equilibrium as before, i.e. minimizing the elastic potential energy. However, this is computationally expensive. Thus, in this work we investigate how to exploit Eqn. (6) also for the simulation of nonlinear bending behaviour. More precisely, we aim for an iterative method, where in each step we update the constant $[EI]_i$ according to $f_{EI}(K_i)$ and solve the energy minimization problem with constant stiffness values.

To obtain correct simulation results, we need to make sure to use consistent bending moments. This means, the bending moment within one iteration step with constant bending stiffness in Eqns. (10) must equal the general bending moment calculated with the first Eqn. in (9). Consequently,

$$[EI]_i \cdot K_i = \int_0^{K_i} f_{EI}(\kappa) d\kappa \tag{11}$$

must hold and yields

$$[EI]_i = \frac{1}{K_i} \cdot \int_0^{K_i} f_{EI}(\kappa) d\kappa. \tag{12}$$

Thus, the stiffness update in each step is done by setting $[EI]_i = g_{EI}(K_i)$, where we define

$$g_{EI}(\kappa) := \frac{1}{\kappa} \int_0^{\kappa} f_{EI}(\xi) d\xi, \tag{13}$$

and, vice versa,

$$f_{EI}(\kappa) = g_{EI}(\kappa) + \kappa \cdot \frac{dg_{EI}(\kappa)}{d\kappa}. \tag{14}$$

The suggested iterative procedure is illustrated in Fig. 5. In each step, a cable state (x_i^m, y_i^m), $i = 0, ..., N$ and $\alpha_{i+1/2}^m$, $i = 0, ..., N-1$, is given, with corresponding curvatures K_i^m and algorithmic local bending stiffness constant $[EI]_i^m = g_{EI}(K_i^m)$ at each vertex. The upper index specifies the iteration step, while the lower index reflects the spatial discretization. By minimizing the elastic potential energy, we find a new equilibrium state (x_i^{m+1}, y_i^{m+1}), $\alpha_{i+1/2}^{m+1}$ and corresponding curvatures K_i^{m+1}. If the curvatures converge, i.e. if $\sum_{i=0}^{N} \delta s_i \cdot |K_i^m - K_i^{m+1}| < tol$, we stop the iteration. Otherwise, we update $[EI]_i^{m+1} = g_{EI}(K_i^{m+1})$ and proceed with the next iteration step. As initial value, we typically use a static equilibrium obtained with constant $[EI]$ for all vertices.

Depending on the slope of the state-dependent bending stiffness characteristic, the iterative method might fail to converge. Therefore, a relaxed update of the bending stiffness values is implemented, leading to convergence also for rather steep slopes. However, details are not discussed in this work.

To illustrate the iterative method, we perform a virtual bending experiment (as described in Section 3.2) where we use a fictive state-dependent bending stiffness characteristic. The characteristic is specified by a natural cubic spline, its shape is determined by three control points (see Fig. 6).

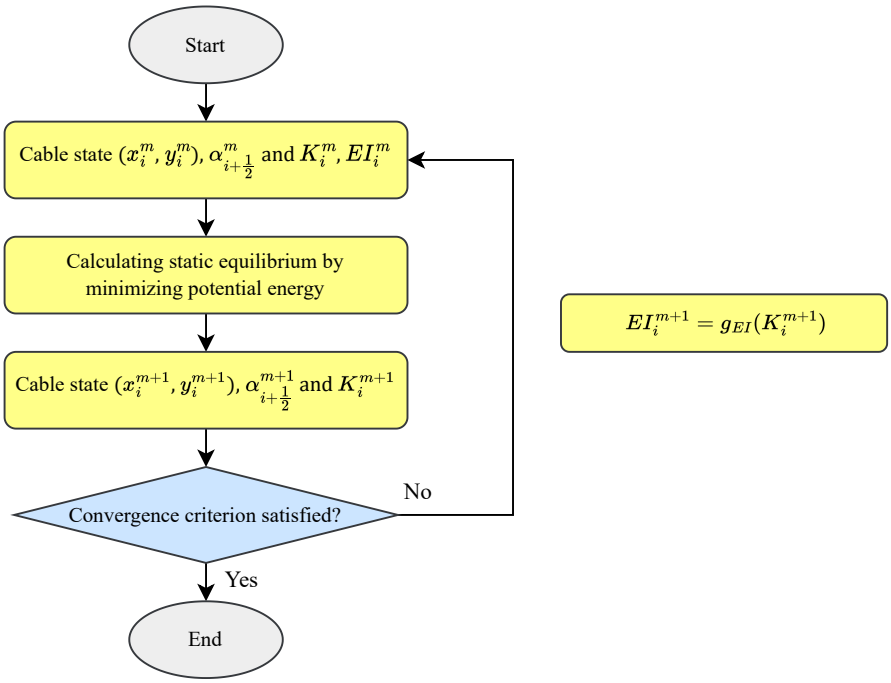

Figure 5: A flow chart for iterative update of the local effective bending stiffness.

In order to validate the iterative method, the solution of an energy minimization with the general bending energy density in Eqns. (9) is performed and serves as reference solution.

The model parameters are shown in Table 1, where $(\hat{\kappa}_0, [\hat{EI}]_0)$, $(\hat{\kappa}_1, [\hat{EI}]_1)$ and $(\hat{\kappa}_2, [\hat{EI}]_2)$ are control points for the spline function to represent the state-dependent bending stiffness characteristic.

$[EA]$ [N]	1000
$[GA]$ [N]	1000
L [m]	0.2
$\hat{\kappa}_0$ [m^{-1}]	0
$\hat{\kappa}_1$ [m^{-1}]	5
$\hat{\kappa}_2$ [m^{-1}]	10
$[\hat{EI}]_0$ [Nm^2]	$1 \cdot 10^{-3}$
$[\hat{EI}]_1$ [Nm^2]	$3 \cdot 10^{-3}$
$[\hat{EI}]_2$ [Nm^2]	$3.5 \cdot 10^{-3}$

Table 1: Simulation parameters.

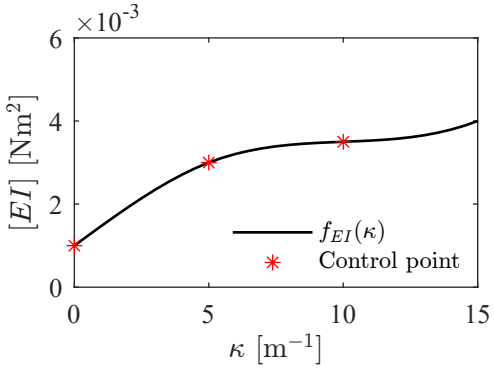

Figure 6: The state-dependent bending stiffness characteristic $f_{EI}(\kappa)$.

First, we only consider one static boundary condition. In Fig. 7, the discrete curvatures K_i are plotted over the arc length s_i. The curvatures in the reference solution are plotted as black dashed curves. The initial state for the iterative method, a circular arc and thus constant curvature, is plotted in solid blue. In the left figure, the first two iteration results are shown

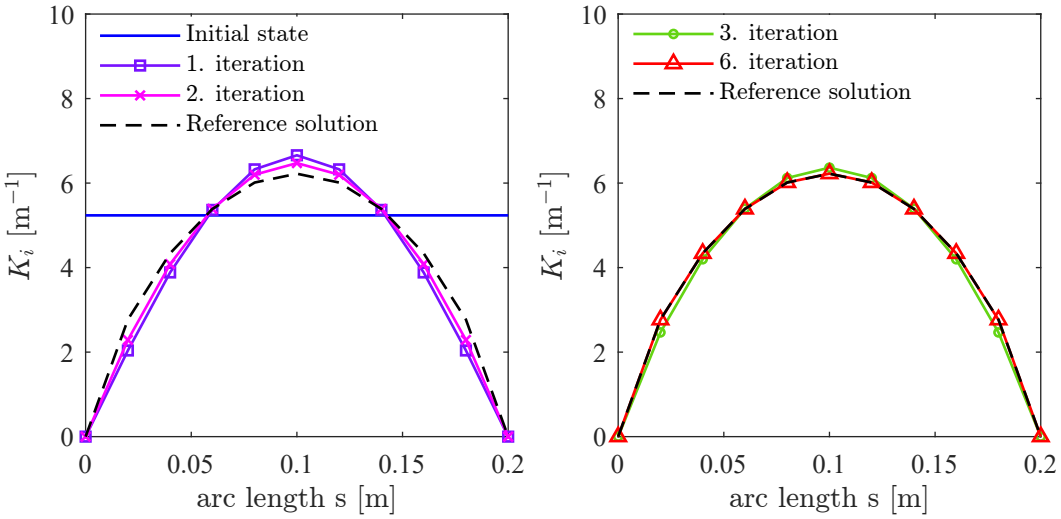

Figure 7: Discrete curvatures in each iteration, compared with the reference solution. As initial state, a circular arc, i.e. constant curvature, is used.

whereas in the right the curvatures after iteration three and six are plotted. One can observe, that after a few iterations, the curvatures in the iterative method converge to the reference solution. In this example, the computational cost for the iterative method is approximately five times lower than for the reference solution, i.e. than solving the energy minimization problem with the bending energy density given in Eqns. (9).

Next, we apply a sequence of static boundary conditions and displace the left mounting point as described in Section 3.2. Fig. 8 shows the horizontal reaction force over the displacement. Since we already start in a bent configuration, the displacement does not start from zero. The plot shows very good agreement between the horizontal reaction force obtained at the fixed end point from iterative method and the reference solution.

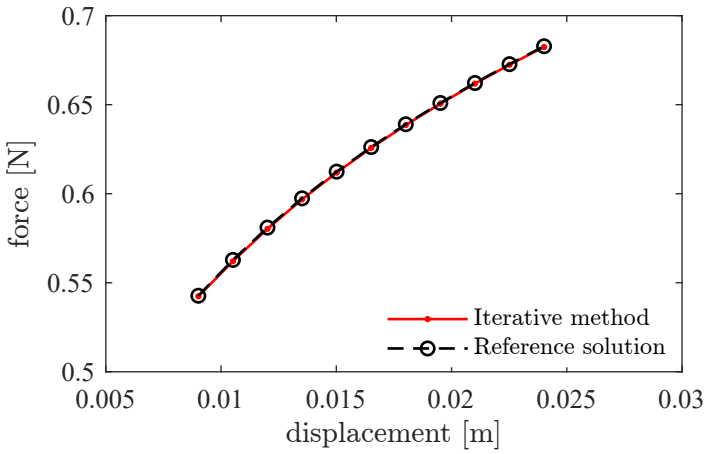

Figure 8: Horizontal reaction force obtained at the fixed end point, resulting from varying displacements.

5 INVERSE PROBLEM

So far, we have assumed given state-dependent bending stiffness characteristics $f_{EI}(\kappa)$ and discussed how to utilize those in our framework of energy minimization with constant bending stiffness. Now, we focus on the question how to determine the characteristic from given measurement results, i.e. the horizontal reaction force. This leads to an inverse problem: find $f_{EI}(\kappa)$ such that $\sum_{j=1}^{J}(F_j^S - F_j^G)^2 < tol$, where the index $j = 1, ..., J$ denotes the given displacements, F_j^S represents the simulated force computed from the current $f_{EI}(\kappa)$ at displacement step j and F_j^G represents the corresponding measured target force.

As previously mentioned, we use a natural cubic spline to represent the state-dependent bending stiffness characteristic. Thus, with that rather general but simple representation, in the inverse problem we find the control points $(\hat{\kappa}_0, [\hat{EI}]_0)$, $(\hat{\kappa}_1, [\hat{EI}]_1)$ and $(\hat{\kappa}_2, [\hat{EI}]_2)$. For simplicity, we assume fixed $\hat{\kappa}_0$, $\hat{\kappa}_1$ and $\hat{\kappa}_2$ and only consider $[\hat{EI}]_0$, $[\hat{EI}]_1$ and $[\hat{EI}]_2$ as optimization variables.

5.1 Inverse problem using virtual measurement data

In order to verify the solution of the inverse problem, we first use virtual measurement data. This means, we simulate the force F_j^G for $j = 1, ..., J$ for a known state-dependent bending stiffness characteristic $f_{EI}(\kappa)$. Thus, one knows the virtually measured force as well as the underlying characteristic $f_{EI}(\kappa)$ and can assess the solution of the inverse problem.

Fig. 9 illustrates the optimization procedure to identify $f_{EI}(\kappa)$. The known state-dependent bending stiffness characteristic, i.e. the reference solution is plotted as black dashed curves. Starting with a constant bending stiffness characteristic, already after the first iteration, $f_{EI}(\kappa)$ is close to the reference solution. In the third iteration, we have a very good agreement. Moreover, Fig. 10 shows the target force F_j^G and the simulated force F_j^S which results from a simulation with the identified state-dependent bending stiffness characteristic after three iterations. This also shows a very good agreement.

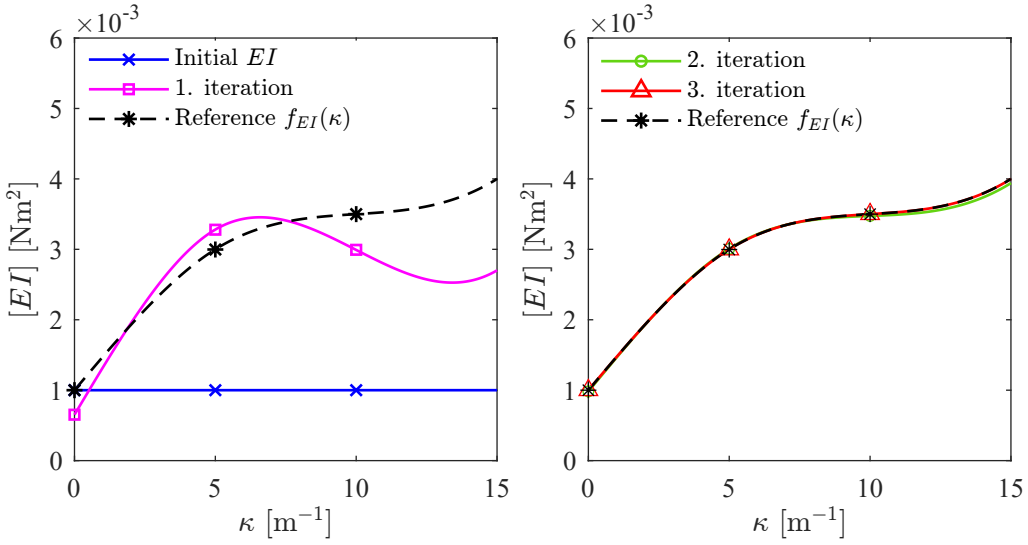

Figure 9: Optimization procedure to identify the $f_{EI}(\kappa)$ using virtual measurement data.

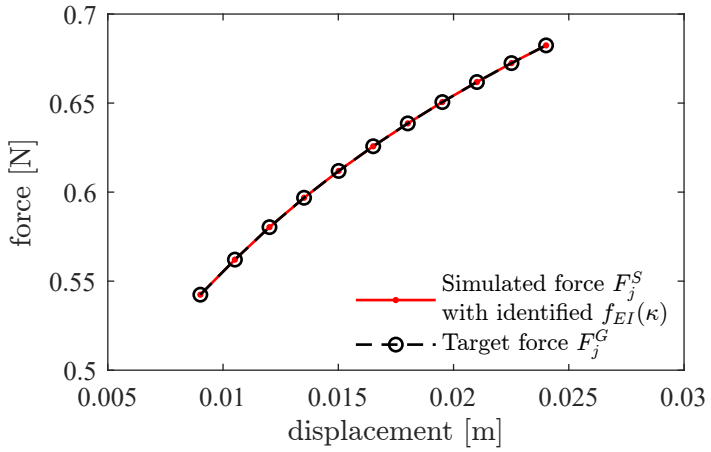

Figure 10: The target force F_j^G and the simulated force F_j^S resulting from a simulation with the identified $f_{EI}(\kappa)$, i.e. after three iterations.

5.2 Inverse problem using real measurement data

Finally, we use real experimental data to solve the inverse problem, i.e. to find $f_{EI}(\kappa)$ for a real cable. The bending test was performed with a cable of diameter 4.6 mm and a free length of 181 mm from clamping to clamping.

Fig. 11b shows the measured force, the force simulated with a constant $[EI]$ (the initial value) and the simulated force according to the identified $f_{EI}(\kappa)$. The identified state-dependent bending stiffness characteristic $f_{EI}(\kappa)$ is shown in Fig. 11a, together with the constant initial characteristic.

The simulated force with the identified stiffness characteristic $f_{EI}(\kappa)$ shows good agreement with the measured force. However, looking on the identified characteristic right from the last control point, the slope looks not very reliable. This is not a surprise, since the maximum curvatures which occur during the test are approx. $11\,\mathrm{m}^{-1}$ and, thus, only very little data is available right from the last control point. Moreover, for small curvatures the $f_{EI}(\kappa)$ becomes negative. Again, a lack of data might be an explanation for that unphysical solution. Another source might be a possible pre-curvature of the cable not considered in the identification of $f_{EI}(\kappa)$. In principle, as described in Section 2, a pre-curvature can simply be added to the rod model. However, identifying the pre-curvature $K_0(s)$ for a real cable specimen is a non-trivial task. In a first observation, we added constant pre-cuvature to the cable model. This clearly influences the solution of the inverse problem (cf. Fig. 12). In a future work, we plan to add the pre-curvature as optimization variable and add the requirement $f_{EI}(\kappa) > 0$ (strict positivity) as a constraint. To this end, another reasonable optimization input might be pictures of the bending line, which are also available from MeSOMICS measurements.

6 CONCLUSION

In this work, we analyzed two aspects for the simulation of nonlinear constitutive behaviour. First, we showed how to efficiently utilize arbitrary state-dependent stiffness characteristics

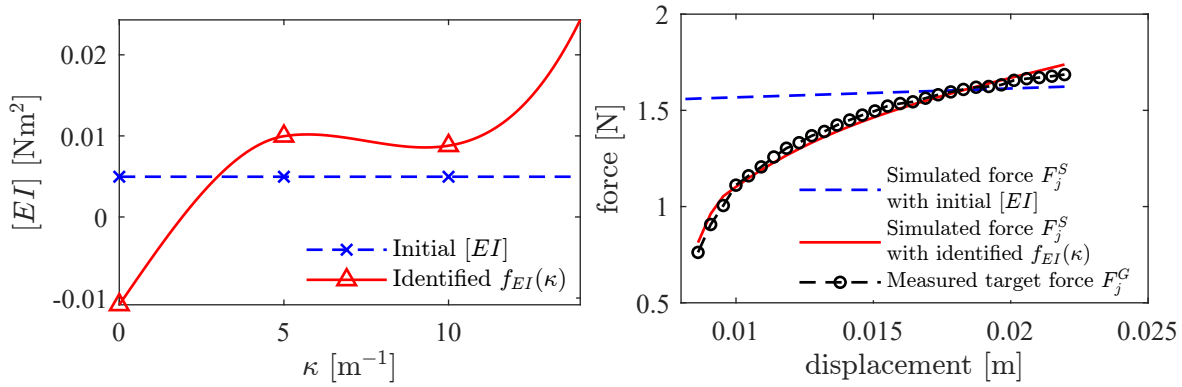

(a) The identified state-dependent bending stiffness characteristic $f_{EI}(\kappa)$.

(b) The simulated force resulting from a initial constant $[EI]$, the simulated force resulting from the identified $f_{EI}(\kappa)$ and the measured force.

Figure 11: Identification of the $[EI]$ characteristic using real measurement data.

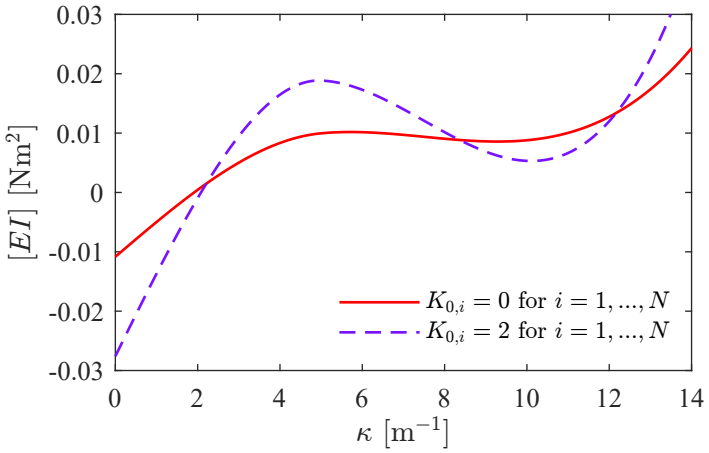

Figure 12: Identified $f_{EI}(\kappa)$ without considering pre-curvature, i.e. vanishing $K_{0,i}$, and with a constant non-zero pre-curvature of $2\,\mathrm{m}^{-1}$.

$f_{EI}(\kappa)$ by means of an iterative method which uses constant stiffness values in each step. The described routine makes use of a very cheap procedure to evaluate the bending energy term. Second, we discussed how to identify state-dependent bending stiffness characteristics $f_{EI}(\kappa)$ from a bending experiment by solving the inverse problem. For both aspects, the current results are promising. Next steps foresee a deeper understanding how pre-curvature influences the solutions of the inverse problem, how to treat pre-curvature as an optimization variable, and constraining the function $f_{EI}(\kappa)$ to the physically admissible range of strictly positive values. Moreover, different cable types will be considered, especially in the inverse problem, to learn more about their qualitative state-dependent bending stiffness characteristic.

REFERENCES

[1] Linn, J., Schneider, F., Dreßler, K., Hermanns, O. Virtual product development and digital validation in automotive industry. In: *Bock, H.G., Küfer, KH., Maass, P., Milde, A., Schulz, V. (eds) German Success Stories in Industrial Mathematics*. Mathematics in Industry (2021) **35**:45-52. Springer, Cham.

[2] Linn, J., Hermansson, T., Andersson, F. and Schneider, F. Kinetic aspects of discrete Cosserat rods based on the difference geometry of framed curves. In: *Valasek, M., et al. (eds) Proceedings of the ECCOMAS Thematic Conference on Multibody Dynamics, Prague, Czech Republic* (2017) 163-176.

[3] Antman, S.S. *Nonlinear problems of elasticity*. Springer, Berlin, (2005).

[4] Reissner, E. On one-dimensional large-displacement finite-strain beam theory. *Studies in applied mathematics* (1973) **52**(2):87-95.

[5] Simo, J.C. A finite strain beam formulation. The three-dimensional dynamic problem. Part I. *Computer methods in applied mechanics and engineering* (1985) **49**(1):55-70.

[6] Dörlich, V., Linn, J., Diebels, S. Flexible beam-like structures - experimental investigation and modeling of cables. In: *Altenbach, H., Jablonski, F., Müller, W., Naumenko, K., Schneider, P. (eds) Advances in Mechanics of Materials and Structural Analysis*. Advanced Structured Materials (2018) **80**:27-46. Springer, Cham.

[7] *MeSOMICS: Measurement System for the Optically Monitored Identification of Cable Stiffnesses*. Homepage: www.mesomics.eu

[8] Papailiou, K.O. On the bending stiffness of transmission line conductors. *IEEE Transactions on Power Delivery* (1997) **12**(4):1576-1588.

[9] Hong, K.J., Der Kiureghian, A. and Sackman, J.L. Bending behavior of helically wrapped cables. *Journal of engineering mechanics* (2005) **131**(5):500-511.

[10] Lang, H., Linn, J., and Arnold, M. Multi-body dynamics simulation of geometrically exact Cosserat rods. *Multibody System Dynamics* (2011) **25**(3):285-312.

[11] Linn, J. Discrete Cosserat rod kinematics constructed on the basis of the difference geometry of framed curves—part I: discrete Cosserat curves on a staggered grid. *J Elast* (2020) **139**:177–236.